Hindawi
Wireless Communications and Mobile Computing
Volume 2022, Article ID 9129436, 8 pages
https://doi.org/10.1155/2022/9129436

Research Article

Cooperative RIS and Relaying IoV Networks: A Deep Study on Position Analysis

Jiaxing Zhu,[1] Guoan Zhang,[1] Yan Jiang,[2] Wei Duan,[1] Jianghong Ou,[3] and Dahua Fan[3]

[1]*School of Information Science and Technology, Nantong University, Nantong 226019, China*
[2]*Engineering Training Center, Nantong University, Nantong 226019, China*
[3]*Starway Communication, Guangzhou Science City, Guangzhou 510663, China*

Correspondence should be addressed to Guoan Zhang; gzhang@ntu.edu.cn

Received 17 March 2022; Revised 20 April 2022; Accepted 13 May 2022; Published 9 June 2022

Academic Editor: Lisheng Fan

In this paper, a hybrid relay- and reconfigurable intelligent surface- (RIS-) assisted cooperative communication system is proposed. Considering the overall user position referring to the reflective RIS, the downlink propagation can be summarized as two cases: for the first case, the mobile user can only be assisted by the relay (on the back of RIS); for the second case, the mobile user will be assisted by both of the RIS and relay. In our proposed system, a novel concept named "balance position" is investigated, which can be used to resolve specific deployment issue of the RIS. Due to the difficulty of obtaining the closed-form expressions of the achievable capacity, we derive the tight upper bound for the channel gain through observing the central limit theorem (CLM) and Jensen's inequality and determine its trend for the mobile user. Numerical results verify the correctness of our analysis and superiority of our proposed scheme. Moreover, for an increasing number of RIS elements, the system capacity will be significantly improved, and the balance position will be far away from RIS.

1. Introduction

With the proposal of the concept of smart city and the development of intelligent transportation system (ITS), people's daily travel has become more convenient and safer. As the cornerstone of the future ITS [1], Internet of Vehicles (IoV) enables the vehicles to maintain robust connection with their surroundings and remote entities, while provides extensive and convenient services for vehicles [2, 3]. Therefore, IoV has higher requirements for delay and throughput. However, due to the complexity of the environment and the mobility of vehicles, how to improve the quality of vehicle communication in the IoV networks has become an enduring problem in the field of wireless transmission research.

Recently, with the continuous development of 5G and B5G, a great number of emerging technologies are proposed to meet the increasing demand for the data traffic, such as massive multiple-input multiple-output (MIMO), deep learning, and mmwave [4, 5]. However, most services deal with the huge transmission by employing large active antennas, which is too expensive and deployed hardly in practical environment. Reconfigurable intelligent surface (RIS) technology receives considerable attentions for its passive reflecting character, moderate price, and flexible deployment. Meanwhile, RIS possesses superiority spectrum efficiency (SE) and great communication coverage, by intelligently reconfiguring the propagation environment of wireless channels [6]. In addition, RIS consists of plenty of reflective elements, which can take advantage of the ultrathin planar structure to independently manage the amplitude and phase of the incoming signals. With deploying the RIS in wireless networks, the traditional random channel state information (CSI) becomes controllable [7, 8].

In the existing IoV networks, relay has been widely deployed and applied, while the technology is relatively mature. Comparing with the conventional relay technology, the RIS embraces significant advantages, and a considerable amount of theoretical researches and applications have been studied recently. In order to compare the performance of the RIS-aided and amplify-and-forward relaying systems, the authors provided a theoretical framework in [9]. Through analyzing the characteristics of the RIS and relay, the author

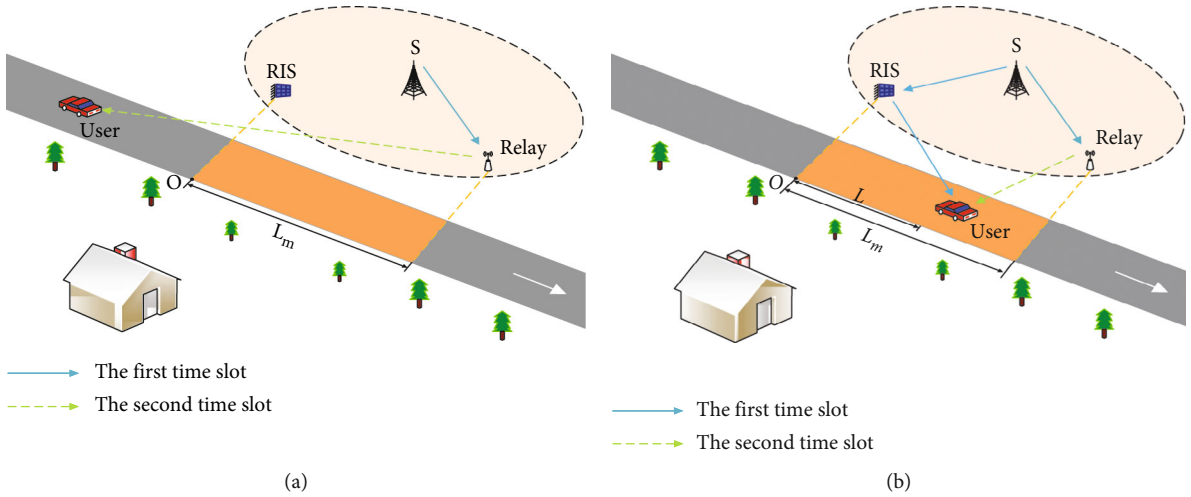

Figure 1: System model: (a) without assistance from RIS, (b) with assistance from RIS.

in [10] elaborated the major differences and similarities. Moreover, when either the relay or RIS is selected to maximize signal-to-noise ratio (SNR), a comparison between the RIS and decode-and-forward (DF) relaying is provided in [11]. Besides, the authors in [12] proposed a novel hybrid relay- and RIS-assisted system to enhance system performance. In [13], a transmission RIS was investigated, which has been a research hotspot recently.

Most of these literatures only focus on the applications of the RIS in a specific environment, e.g., fixed user locations. However, focusing on the current smart city, the capacity of information interaction for mobile devices and vehicular applications is breathtakingly increasing among IoV networks, and a great number of novel technologies, such as mobile edge computing (MEC), are proposed to resolve the huge data traffic [14, 15]. Motivated by above observations, it is promising to study the cooperative RIS and relay jointly assisted IoV networks. Considering the actual situation that the RIS should assist with the existing relay in the initial application, this paper proposes a cooperative reflection RIS and relaying communication system with mobile users, where two scenarios are considered: (i) the mobile user is only assisted by the relay (on the back of RIS); (ii) the mobile user is assisted by both of the RIS and relay. The main contributions of this paper are summarized as follows.

(i) A novel reflective RIS- and relay-assisted cooperative system is investigated, in which the overall position of the mobile user is considered. To clarify the deployment of RIS, a concept of "balance position" is provided, i.e., the equivalent achievable capacity by the RIS and relay

(ii) For the ideal RIS case with optimal reflection, we derive closed-form expressions of the channel gain by exploiting the Jensen's inequality and central limit theorem. The tight upper bound on the achievable capacity is also studied with its trend for mobile user

(iii) Numerical results verify the accuracy of the theoretical analysis revealing the achievable capacity increases firstly and then decreases with the movement of users in the system. Then, the effect of the deployment distance between the RIS and relay on the system is discussed in limited resource environment. The results show that if the deployment distance is too close, the performance of relay will be always better than the RIS

2. System Model

In this section, a hybrid RIS- and relay-assisted communication system is proposed, which is including a source (S), a relay (R), an RIS (I) with N elements, as well as a mobile user (D), as shown in Figure 1. The half-duplex relay adopting the DF protocol and reflective RIS assist the information transfer from S to D, due to the limited coverage of S [16]. In the actual scenes, without loss of generality, the user will enter the communication range from the left or right side. Since these two scenes are similar, for simplicity, we only consider that the activity direction of D is from the back of the RIS towards to the relay. Clearly, there are two possible cases: (i) the user is only assisted by the relay (on the back of RIS); (ii) the user is assisted by both of the RIS and relay (including scenarios of that the user is near to the RIS but far from the relay, and the user is closed to the relay but far from the RIS). Specifically, as shown in Figure 1, for the first case, D enters the coverage of R from the blind sight of I, resulting in that D only receives the signals from the relay. Then, when D moves into the orientation of I, it simultaneously receives the signals from the RIS and relay. For simplicity, we further consider that the RIS and relay will not forward the signals to each other. In the following sections, we denote the channels $S \longrightarrow I$, $S \longrightarrow R$, $I \longrightarrow D$, and $R \longrightarrow D$ as $h_{\mathrm{SI}} \in \mathbb{C}^N$, $h_{\mathrm{SR}} \in \mathbb{C}$, $h_{\mathrm{ID}} \in \mathbb{C}^N$, and $h_{\mathrm{RD}} \in \mathbb{C}$, satisfying independent Rayleigh distributions.

2.1. Only Relay-Assisted Transmission. In this case, S transmits signals to R and I. Due to the blind region of I, D can only receive signals from R, as shown in Figure 1(a). Specifically, according to the half-duplex DF protocol, the transmission from S to D involves two time slots. During the first time slot, S transmits the signal to R, and the received signal at R can be expressed as

$$y_{1,R} = h_{\mathrm{SR}}\sqrt{P}s + n_{1,R}, \tag{1}$$

where $n_{1,R} \sim \mathscr{CN}(0, \sigma^2)$ means the received additive white Gaussian noise (AWGN) at R, P means the transmit power, and s means the transmitted signal with $E[|s|^2] = 1$.

During the second time slot, R decodes and forwards s to D. Therefore, the received signal at D can be given as

$$y_{2,D} = h_{\mathrm{RD}}\sqrt{P}s + n_{2,D}, \tag{2}$$

where $n_{2,D} \sim \mathscr{CN}(0, \sigma^2)$ means the AWGN at D. Denoting $P/\sigma^2 = \rho$ and adopting the maximum ratio combining (MRC), the achievable rate at D can be obtained from [17]

$$\mathscr{R}_{\mathrm{DF}} = \frac{1}{2}\log_2\left(1 + \rho \min\left(|h_{\mathrm{SR}}|^2, |h_{\mathrm{RD}}|^2\right)\right), \tag{3}$$

where 1/2 means the transmission involving two time slots.

2.2. Relay- and RIS-Assisted Transmission. In this case, D enters the reflection orientation of I, in which it can receive the signals reflected by I and forwarded from R. Note that I is embedded with N discrete elements, and the size of each element is incomparable with the wavelength. Therefore, it can flexibly scatter the incident signal with almost constant gain in all directions of interest. In this manner, the signal reflected by I can be expressed as

$$y_{\mathrm{RIS}} = \sqrt{P}\left(\mathbf{h}_{\mathrm{SI}}^{\mathrm{T}}\boldsymbol{\Theta}\mathbf{h}_{\mathrm{IR}}\right)s + n_I, \tag{4}$$

where $n_I \sim \mathscr{CN}(0, \sigma^2)$ means the AWGN at I, and $\boldsymbol{\Theta} = \mathrm{diag}\left(\eta_1 e^{j\theta_1}, \cdots, \eta_N e^{j\theta_N}\right)$ denotes the reflection matrix of the RIS, where $\eta_i \in [0, 1]$ and $\theta_i \in [0, 2\pi]$, respectively, denote the amplitude attenuation and phase-shift of the ith element, for $i = [1, 2, \cdots, N]$. Therefore, the received SNR at I can be obtained from [12]

$$\gamma_{\mathrm{RIS}} = \rho\left|\sum_{i=1}^{N}\eta_i e^{j\theta_i}[\mathbf{h}_{\mathrm{SI}}]_i[\mathbf{h}_{\mathrm{ID}}]_i\right|^2. \tag{5}$$

Based on Shannon theory, the capacity of RIS-assisted scenario is calculated by

$$\mathscr{R}_{\mathrm{RIS}} = \log_2(1 + \gamma_{\mathrm{RIS}}) = \log_2\left(1 + \rho\left|\sum_{i=1}^{N}\eta_i e^{j\theta_i}[\mathbf{h}_{\mathrm{SI}}]_i[\mathbf{h}_{\mathrm{ID}}]_i\right|^2\right). \tag{6}$$

Since the received signal at D from R is similar to the only relay-assisted transmission case previous subsection, we omit it here. Combining Equations (3) and (6), the achievable sum-rate at D is finally expressed as

$$\mathscr{R}_{\mathrm{sum}} = \mathscr{R}_{\mathrm{RIS}} + \mathscr{R}_{\mathrm{DF}}. \tag{7}$$

The practical transmission of the relay should consume two time slots. During the second time slot, the relay decodes and forwards the signal to D. Meanwhile, the RIS reflects the signal received from S again. Therefore, the achievable sum-rate at D of two time slots can be expressed as $2\mathscr{R}_{\mathrm{sum}}$. Since the sum-rate has the linear relationship with the time slot, and the subsequent analysis focuses on the trend of $\mathscr{R}_{\mathrm{sum}}$, the sum-rate of one time slot is analyzed in the following.

3. Performance Analysis for Proposed Scheme

In this section, considering the number of the RIS elements and distances from D to I and R, the influence of D in different positions on its achievable rate is discussed.

3.1. Maximal Achievable Rates for Proposed System. For simplicity, we assume that the perfect CSI is obtained to realize the ideal passive beamforming at I [18]. It is the optimal phase shift that align the signal reflected by RIS with the user in the proposed system [7]. Therefore, it is clear that the optimal γ_{RIS} can be obtained when $\theta_i = 0$. Meanwhile, it is assumed that the phase shifts can be controlled to change continuously to obtain the optimal phase shift, while the reflection amplitude of all elements is assumed to be η. Accordingly, optimal γ_{RIS} can be equivalently simplified as

$$\gamma_{\mathrm{RIS}} = \rho\left|\sum_{i=1}^{N}\eta_i e^{j\theta_i}[\mathbf{h}_{\mathrm{SI}}]_i[\mathbf{h}_{\mathrm{ID}}]_i\right|^2 = \rho\left|\sum_{i=1}^{N}\eta[\mathbf{h}_{\mathrm{SI}}]_i[\mathbf{h}_{\mathrm{ID}}]_i\right|^2. \tag{8}$$

Through observing the statistical characteristics of the CSI, we derive the ergodic capacity of our scheme, following the Jensen's inequality as

$$\mathbb{E}[\log_2(1 + v)] \le \log_2(1 + \mathbb{E}[v]). \tag{9}$$

The channels are denoted as $h_j = g_j d_j^{-\alpha/2}, j \in \{\mathrm{SR}, \mathrm{RD}\}$, and $\mathbf{h}_k = \mathbf{g}_k d_k^{-\alpha/2}, k \in \{\mathrm{SI}, \mathrm{ID}\}$, in which $g_j \in \mathbb{C}$ and $\mathbf{g}_k \in \mathbb{C}^N$ stand for the complex Gaussian fading factors following $\mathscr{CN}(0, 1)$, and d and α, respectively, denote the distance and path-loss exponent for the corresponding channels.

Note $\sqrt{\beta_j} = |h_j|$, $\sqrt{\beta_{\mathrm{SID}}} = \eta/N\sum_{i=1}^{N}|[\mathbf{h}_{\mathrm{SI}}]_i[\mathbf{h}_{\mathrm{ID}}]_i|$, where β_j means exponentially distributed with $\mathbb{E}[\beta_j] = d_j^{-\alpha}$. Morever, for the RIS with plenty of elements, β_{SID} follows a noncentral chi-square distribution with $\mathbb{E}[\beta_{\mathrm{SID}}] = \eta^2[\pi^2 + (1/N)(16 - \pi^2)]/16 d_{\mathrm{SI}}^{\alpha} d_{\mathrm{ID}}^{\alpha}$ [19]. With these observations, the expectation of the upper bound for γ_{RIS} can be derived as

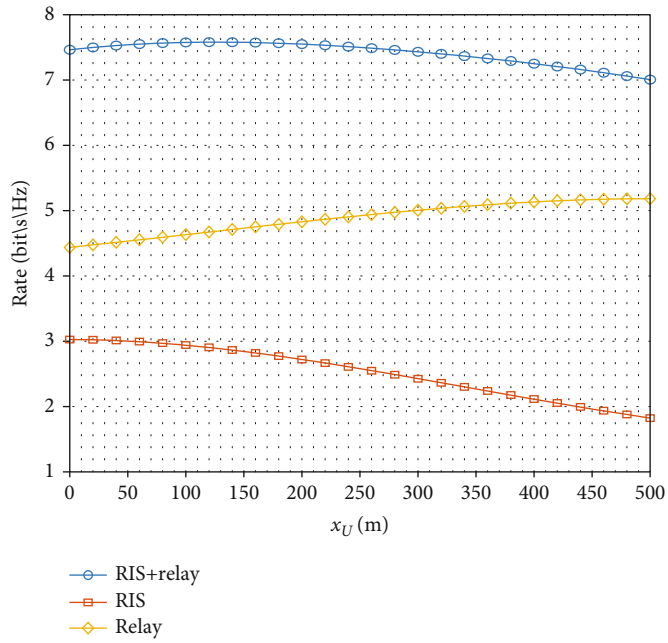

Figure 2: Achievable rate of user versus user position in our proposed system.

$$\mathbb{E}[\tilde{\gamma}_{\mathrm{RIS}}] = \mathbb{E}\left[\rho\left(N\sqrt{\beta_{\mathrm{SID}}}\right)^2\right] = \rho N^2 \mathbb{E}[\beta_{\mathrm{SID}}] = \frac{1}{16}\rho d_{\mathrm{SI}}^{-a} d_{\mathrm{IR}}^{-a}\eta^2 N\left(16 + (N-1)\pi^2\right). \tag{10}$$

Finally, the upper bound ergodic capacity of our scheme can be obtained from

$$\tilde{\mathscr{R}}_{\mathrm{sum}} = \tilde{\mathscr{R}}_{\mathrm{DF}} + \tilde{\mathscr{R}}_{\mathrm{RIS}} \le \frac{1}{2}\log_2\left(1 + \min\left(\mathbb{E}[\beta_{\mathrm{SR}}], \mathbb{E}[\beta_{\mathrm{RD}}]\right)\right) + \log_2\left(1 + \mathbb{E}[\tilde{\gamma}_{\mathrm{RIS}}]\right). \tag{11}$$

As shown in Figures 1(a) and 1(b), the intersection of I projection and D motion route is represented as O, the distance between the location of I and the point O is denoted by d, the distance relative to point O is set to L, and the distance between I and R is denoted to L_m. By this way, the distances from D to I and R can be, respectively, given as $d_{\mathrm{ID}} = \left(L^2 + d^2\right)^{1/2}$ and $d_{\mathrm{RD}} = \left((L_m - L)^2 + d^2\right)^{1/2}$. With above results and Equation (11), $\tilde{\mathscr{R}}_{\mathrm{sum}}$ can be derived as

$$\tilde{\mathscr{R}}_{\mathrm{sum}}(L) = \frac{1}{2}\log_2\left[1 + \rho\min\left(d_{\mathrm{SR}}^{-\alpha}, \left((L_m - L)^2 + d^2\right)^{-\alpha/2}\right)\right] + \log_2\left[1 + \frac{1}{16}\rho\eta^2 d_{\mathrm{SI}}^{-\alpha} N\left(16 + (N-1)\pi^2\right)\left(L^2 + d^2\right)^{-\alpha/2}\right]. \tag{12}$$

In order to discuss the characteristics of $\tilde{\mathscr{R}}_{\mathrm{sum}}$, the first-order derivation of $\tilde{\mathscr{R}}_{\mathrm{sum}}$ is obtained, with respect to L. Due to the complexity of mathematical manipulation, the function is divided into two cases for better analysis. For $d_{\mathrm{RD}} \ge d_{\mathrm{SR}}$, the first-order derivation of $\tilde{\mathscr{R}}_{\mathrm{sum_a}}$ can be derived as

$$\widetilde{\mathscr{R}}'_{\mathrm{sum_a}} = \frac{\alpha\rho\left((L_m - L)^2 + d^2\right)^{-(\alpha/2)-1}(L_m - L)}{2\ln 2\left(1 + \rho\left((L_m - L)^2 + d^2\right)^{-\alpha/2}\right)} + \underbrace{\frac{-\alpha\rho\eta^2 d_{\mathrm{SI}}^{-\alpha} N\left(16 + (N-1)\pi^2\right)L\left(L^2 + d^2\right)^{-(\alpha/2)-1}}{16\ln 2\left[1 + 1/16\rho\eta^2 d_{\mathrm{SI}}^{-\alpha} N(16 + (N-1)\pi^2)\left(L^2 + d^2\right)^{-\alpha/2}\right]}}_{A}. \tag{13}$$

For $d_{\mathrm{RD}} \le d_{\mathrm{SR}}$, due to that the relay forwarded signal is not related to L, the first-order derivation derivative of $\tilde{\mathscr{R}}_{\mathrm{sum_b}}$ can be simply written as

$$\widetilde{\mathscr{R}}'_{\mathrm{sum_b}} = A. \tag{14}$$

From Equations (13) and (14), it is clear that, for $L = 0$, the first derivation of $\tilde{\mathscr{R}}_{\mathrm{sum}_a}$ will always be greater than 0, and the first derivation of $\tilde{\mathscr{R}}_{\mathrm{sum}_b}$ is a negative result. Therefore, it can be concluded that $\mathscr{R}_{\mathrm{RIS}}$ is a monotonically increasing function, while $\mathscr{R}_{\mathrm{DF}}$ is a monotonically subtraction function. Hence, according to the existence theorem of zero points, it is possible to find an optimal L^* maximizing the system capacity. Due to the difficulty of obtaining the closed-form solution of this optimal value, the numerical solution of the optimal value under specific conditions is obtained in following simulation results.

3.2. Balance Position of the Relay and RIS. Considering some actual scenarios, e.g., limited resources, the RIS and relay are not allowed to serve users simultaneously. Balance position

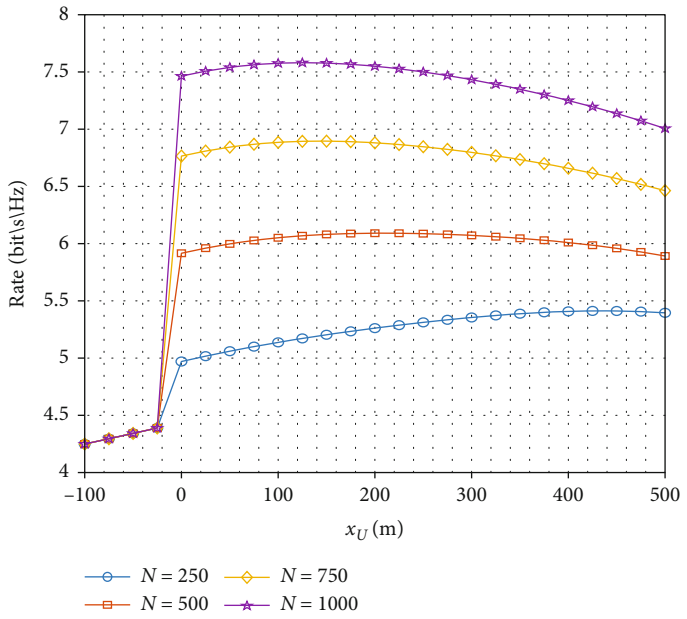

Figure 3: Achievable rate of user versus user position in our proposed system.

denotes the position where the equivalent achievable capacity can be achieved by the RIS and relay. The significance of the balance position is that a more efficient communication mode can be selected according to position of the user relative to the balance position.

From Equation (10), it is clear that $\tilde{\gamma}_{\mathrm{RIS}}$ is an increasing function of N. If there is a balance position, the reflection element N should satisfy the following constraints:

$$\mathscr{R}_{\mathrm{DF}_{\min}} \le \mathscr{R}_{\mathrm{RIS}}(N) \le \mathscr{R}_{\mathrm{DF}_{\max}}. \tag{15}$$

As mentioned above, $\mathscr{R}_{\mathrm{DF}}$ is an increasing function of L. Therefore, from Equation (6), when $L = 0$, $\mathscr{R}_{\mathrm{DF}_{\min}} = 1/2 \log_2(1 + \rho \min(d_{\mathrm{SR}}^{-\alpha}, (L_m^2 + d^2)^{-\alpha/2}))$; meanwhile, for $L = L_m$, $\mathscr{R}_{\mathrm{DF}_{\max}} = 1/2 \log_2(1 + \rho \min(d_{\mathrm{SR}}^{-\alpha}, d^{-\alpha}))$. Therefore, Equation (15) can be expressed as

$$\begin{aligned}
&\frac{1}{2}\log_2(1+\rho\min(d_{\mathrm{SR}}^{-\alpha}, d^{-\alpha}))\\
&\ge \log_2\left[1+\frac{1}{16}\rho\eta^2 d_{\mathrm{SI}}^{-\alpha} N\left(16+(N-1)\pi^2\right)\left(L^2+d^2\right)^{-\alpha/2}\right]\\
&\ge \frac{1}{2}\log_2\left(1+\rho\min\left(d_{\mathrm{SR}}^{-\alpha}, \left(L_m^2+d^2\right)^{-\alpha/2}\right)\right).
\end{aligned} \tag{16}$$

Through inequality transformation, Equation (16) is simplified to the inequality about N as

$$\begin{aligned}
N \ge\ & \frac{1}{2d_{\mathrm{SI}}^{-\alpha}\rho\eta^2\pi^2}\sqrt{d_{\mathrm{SI}}^{-\alpha}\rho\eta^2\left(256d_{\mathrm{SI}}^{-\alpha}\rho\eta^2 + d_{\mathrm{SI}}^{-\alpha}\rho\eta^2\pi^4 + 32\pi^2\left(2d^{\alpha}\left(\left(1+\rho\min\left(d_{\mathrm{SR}}^{-\alpha}, \left(L_m^2+d^2\right)^{-\alpha/2}\right)\right)^{1/2}-1\right) - d_{\mathrm{SI}}^{-\alpha}\rho\eta^2\right)\right)}\\
&+ \frac{d_{\mathrm{SI}}^{-\alpha}\left(-16+\pi^2\right)\rho\eta^2}{2d_{\mathrm{SI}}^{-\alpha}\rho\eta^2\pi^2},
\end{aligned} \tag{17}$$

$$\begin{aligned}
N \le\ & \frac{1}{2d_{\mathrm{SI}}^{-\alpha}\rho\eta^2\pi^2}\sqrt{d_{\mathrm{SI}}^{-\alpha}\rho\eta^2\left(256d_{\mathrm{SI}}^{-\alpha}\rho\eta^2 + d_{\mathrm{SI}}^{-\alpha}\rho\eta^2\pi^4 + 32\pi^2\left(2\left(d^2+L_m^2\right)^{\alpha/2}\left(\left(1+\rho\min\left(d_{\mathrm{SR}}^{-\alpha}, d^{-\alpha}\right)\right)^{1/2}-1\right) - d_{\mathrm{SI}}^{-\alpha}\rho\eta^2\right)\right)}\\
&+ \frac{d_{\mathrm{SI}}^{-\alpha}\left(-16+\pi^2\right)\rho\eta^2}{2d_{\mathrm{SI}}^{-\alpha}\rho\eta^2\pi^2}.
\end{aligned} \tag{18}$$

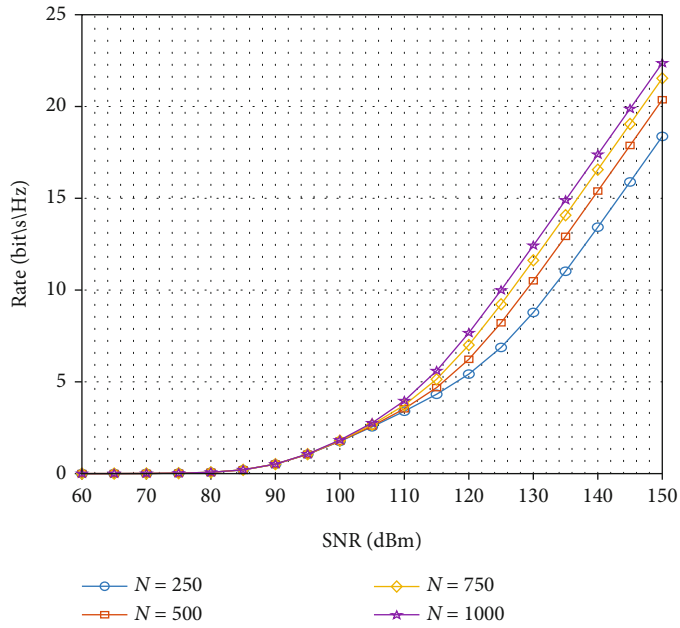

Figure 4: Achievable rate of user versus SNR in our proposed system.

To figure out where the balance position is, the problem about L is proposed as

$$\log_2\left[1+\frac{1}{16}\rho\eta^2 d_{\mathrm{SI}}^{-\alpha}N\left(16+(N-1)\pi^2\right)\left(L^2+d^2\right)^{-\alpha/2}\right] = \frac{1}{2}\log_2\left[1+\rho\min\left(d_{\mathrm{SR}}^{-\alpha},\left((L_m-L)^2+d^2\right)^{-\alpha/2}\right)\right]. \tag{19}$$

According to the knowledge of information theory, the achievable rate of the relay forwarding is limited by the less value of the two-stage channel gain. Since the position of the user is changing, and the channel relayed to user changes with the user's movement, the balance position is discussed in two cases.

Discussion 1. If $d_{\mathrm{SR}} \geq d_{\mathrm{RD}}$, Equation (19) can be further expressed as

$$\log_2\left[1+\frac{1}{16}\rho\eta^2 d_{\mathrm{SI}}^{-\alpha}N\left(16+(N-1)\pi^2\right)\left(L^2+d^2\right)^{-\alpha/2}\right] = \frac{1}{2}\log_2\left(1+\rho d_{\mathrm{SR}}^{-\alpha}\right). \tag{20}$$

It is easy to see that these exists two solutions for Equation (20). Omitting the negative result, the optimal result of L for Equation (20) is

$$L^* = \left(\left(\frac{16\left(\left(1+\rho d_{\mathrm{SR}}^{-\alpha}\right)^{1/2}-1\right)}{\rho\eta^2 d_{\mathrm{SI}}^{-\alpha}N(16+(N-1)\pi^2)}\right)^{-2/\alpha}-d^2\right)^{1/2}. \tag{21}$$

Discussion 2. If $d_{\mathrm{SR}} \leq d_{\mathrm{RD}}$, Equation (19) can be expressed as

$$\log_2\left[1+\frac{1}{16}\rho\eta^2 d_{\mathrm{SI}}^{-\alpha}N\left(16+(N-1)\pi^2\right)\left(L^2+d^2\right)^{-\alpha/2}\right] = \frac{1}{2}\log_2\left(1+\rho\left((L_m-L)^2+d^2\right)^{-\alpha/2}\right). \tag{22}$$

Since the optimal result of L in Equation (22) is quite difficult to obtain, we turn to verify it by Monte Carlo simulation in following numerical results.

4. Numerical Results and Analysis

In this section, we perform simulation to verify the achievable rate with the mobile user and the influence of N for our proposed system. By means of the simulation results, the effect of the deployment distance between the RIS and relay on the balance position is also analyzed.

Similar to [20], the 3GPP urban micro (UMi) under 3 GHz operating frequency is used to model the channel gains [21], which is the typical channel gain with distance as the parameter. Hence, the path loss model can be given as

$$\beta(L)[\mathrm{dB}] = G_{\mathrm{t}} + G_{\mathrm{r}} - 37.5 - 22\log_{10}(L/1\mathrm{m}), \tag{23}$$

where G_{t} and G_{r}, respectively, stand for the antenna gains at the transmitter and receiver. The simulation setup in Figure 1 is considered. For simplicity, following locations of each node is considered: $(x_S, y_S) = (250,600)$, $(x_I, y_I) = (0,400)$, and $(x_R, y_R) = (500,400)$. Meanwhile, the user moves right along the x-axis; the coordinates of the mobile user are expressed as $(x_D, 0)$. We assume that the mobile user is equipped with a 0 dBi omnidirectional antenna; other nodes have 5 dBi antenna gain. Moreover, it is assumed that $P = 500$ W, $B = 10$ MHz, and the noise power is −94 dBm.

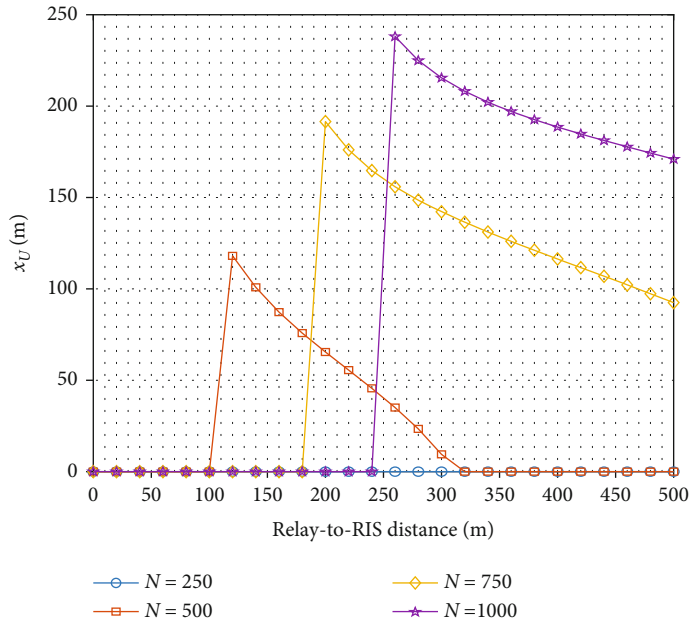

Figure 5: Balance position versus distance between the RIS and relay.

4.1. Achievable Rates of the Proposed Hybrid Scheme. Figure 2 demonstrates the capacity change of each link in the proposed system for $N = 1000$. $d_{IR} = 50$ m, and $N = 50$. It is easy to see that, with the movement of the user, the capacity of the RIS-assisted link decreases monotonically, while that the capacity corresponding to relay-assisted link is improved. Specifically, there exists one point maximizing the system capacity, which is consistent with our theoretical analysis. Figure 3 demonstrates the change of achievable rate under different N when the user enters the system from $(-100,0)$, for $N \in \{250,500,750,1000\}$. It is clear that the achievable rate increases before user enters the reflection region of the RIS. Once entering the RIS coverage, with the reflected signals from the RIS, the achievable rate will be significantly increased verifying the trend in Figure 2. Specifically, the position where the maximum rate occurs is also affected by N. Figure 4 demonstrates the change of achievable rate at different SNR under different N, for x_D=100 m. It is clear that when the channel fading is sufficient large, a greater N results in a more superior performance for high SNR. In conclusion, on the premise that the actual technical conditions permit, a greater N results in a better performance in terms of capacity.

4.2. Balance Position. In the proposed system, when the mobile user moves to the left of the balance position and only one node can be selected to maximize the SNR, the performance of the selecting relay is better than that of the RIS. Otherwise, the RIS should be selected. The influence of changing the distance between the RIS and relay (d_{IR}) on the balance position is discussed. We set the ordinate of the RIS and relay as 200 m, and the source ordinate as 300 m, while adjusting d_{IR} from 0 m to 500 m, the relationship between the balance positions and d_{IR} is illustrated in Figure 5. Clearly, the balance position will be close to the RIS due to the increasing d_{IR} and decreasing N. The points falling on the x-axis indicates that there is no balance position in these conditions. For $N = 250$, there is no balance position, since N is not enough to satisfy the conditions of Equations (17) and (18). Therefore, when considering the practical application scenario, especially for the one with limited transmit power, it is also necessary to select the appropriate deployment distance. Otherwise, the effect of the RIS may always be worse than that of relay due the passive reflection for RIS.

5. Conclusion

Focusing on the reflective RIS, a hybrid relay- and RIS-assisted cooperative IoV communication system was proposed, with the considering of overall mobile user positions. In addition, a novel balance position concept for such system is investigated to resolve specific deployment issue of the RIS. The tight upper bound of the capacity for the mobile user is derived. By means of numerical results, our proposed system show its superiority, especially for an increasing number of RIS elements. Moreover, the balance position will be far away from the RIS for a greater N.

Data Availability

No data were used to support this study.

Conflicts of Interest

The authors declare that they have no conflicts of interest.

Acknowledgments

This work was supported in part by the National Natural Science Foundation of China under Grant 61801249 and Grant 61971245 and the Postgraduate Research & Practice Innovation Program of Jiangsu Province under Grant KYCX21-3086.

References

[1] J. Wang, C. Jiang, K. Zhang, T. Q. S. Quek, Y. Ren, and L. Hanzo, "Vehicular sensing networks in a smart city: principles, technologies and applications," *IEEE Wireless Communications*, vol. 25, no. 1, pp. 122–132, 2018.

[2] A. Al-Hilo, M. Samir, M. Elhattab, C. Assi, and S. Sharafeddine, "Reconfigurable intelligent surface enabled vehicular communication: joint user scheduling and passive beamforming," *IEEE Transactions on Vehicular Technology*, vol. 71, no. 3, pp. 2333–2345, 2022.

[3] J. Wang, C. Jiang, Z. Han, Y. Ren, and L. Hanzo, "Internet of Vehicles: sensing-aided transportation information collection and diffusion," *IEEE Transactions on Vehicular Technology*, vol. 67, no. 5, pp. 3813–3825, 2018.

[4] B. Lin, F. Gao, S. Zhang, T. Zhou, and A. Alkhateeb, "Deep learning based antenna selection and CSI extrapolation in massive MIMO systems," *IEEE Transactions on Wireless Communications*, vol. 20, no. 11, pp. 7669–7681, 2021.

[5] F. Gao, B. Lin, C. Bian, T. Zhou, J. Qian, and H. Wang, "FusionNet: enhanced beam prediction for mmWave communications using sub-6 GHz channel and a few pilots," *IEEE Transactions on Communications*, vol. 69, no. 12, pp. 8488–8500, 2021.

[6] Q. Wu and R. Zhang, "Towards smart and reconfigurable environment: intelligent reflecting surface aided wireless network," *IEEE Communications Magazine*, vol. 58, no. 1, pp. 106–112, 2020.

[7] Q. Wu, S. Zhang, B. Zheng, C. You, and R. Zhang, "Intelligent reflecting surface-aided wireless communications: a tutorial," *IEEE Transactions on Communications*, vol. 69, no. 5, pp. 3313–3351, 2021.

[8] Q. Wu and R. Zhang, "Beamforming optimization for wireless network aided by intelligent reflecting surface with discrete phase shifts," *IEEE Transactions on Communications*, vol. 68, no. 3, pp. 1838–1851, 2020.

[9] A. A. Boulogeorgos and A. Alexiou, "Performance analysis of reconfigurable intelligent surface-assisted wireless systems and comparison with relaying," *IEEE Access*, vol. 8, pp. 94463–94483, 2020.

[10] M. Di Renzo, K. Ntontin, J. Song et al., "Reconfigurable intelligent surfaces vs. relaying: differences, similarities, and performance comparison," *IEEE Open Journal of the Communications Society*, vol. 1, pp. 798–807, 2020.

[11] J. Ye, A. Kammoun, and M.-S. Alouini, "Spatially-distributed RISs vs relay-assisted systems: a fair comparison," *IEEE Open Journal of the Communications Society*, vol. 2, pp. 799–817, 2021.

[12] Z. Abdullah, G. Chen, S. Lambotharan, and J. A. Chambers, "A hybrid relay and intelligent reflecting surface network and its ergodic performance analysis," *IEEE Wireless Communications Letters*, vol. 9, no. 10, pp. 1653–1657, 2020.

[13] S. Zhang, H. Zhang, B. Di, Y. Tan, Z. Han, and L. Song, "Beyond intelligent reflecting surfaces: reflective-transmissive metasurface aided communications for full-dimensional coverage extension," *IEEE Transactions on Vehicular Technology*, vol. 69, no. 11, pp. 13905–13909, 2020.

[14] W. Duan, J. Gu, M. Wen, G. Zhang, Y. Ji, and S. Mumtaz, "Emerging technologies for 5G-IoV networks: applications, trends and opportunities," *IEEE Network*, vol. 34, no. 5, pp. 283–289, 2020.

[15] W. Duan, X. Gu, M. Wen, Y. Ji, J. Ge, and G. Zhang, "Resource management for intelligent vehicular edge computing networks," *IEEE Transactions on Intelligent Transportation Systems*, pp. 1–12, 2021.

[16] D. Lee and J. H. Lee, "Outage probability of decode-and-forward opportunistic relaying in a multicell environment," *IEEE Transactions on Vehicular Technology*, vol. 60, no. 4, pp. 1925–1930, 2011.

[17] J. N. Laneman, D. N. C. Tse, and G. W. Wornell, "Cooperative diversity in wireless networks: efficient protocols and outage behavior," *IEEE Transactions on Information Theory*, vol. 50, no. 12, pp. 3062–3080, 2004.

[18] Q. Wu and R. Zhang, "Intelligent reflecting surface enhanced wireless network via joint active and passive beamforming," *IEEE Transactions on Wireless Communications*, vol. 18, no. 11, pp. 5394–5409, 2019.

[19] E. Basar, M. D. Renzo, J. D. Rosny, M. Debbah, M.-S. Alouini, and R. Zhang, "Wireless communications through reconfigurable intelligent surfaces," *IEEE Access*, vol. 7, pp. 116753–116773, 2019.

[20] E. Bjornson, O. Ozdogan, and E. G. Larsson, "Intelligent reflecting surface versus decode-and-forward: how large surfaces are needed to beat relaying?," *IEEE Wireless Communications Letters*, vol. 9, no. 2, pp. 244–248, 2020.

[21] "Further Advancements for E-UTRA Physical Layer Aspects(-Release 9)," *3GPP Technical Specification, TR 36.814*, vol. 4, no. 1, 2009http://www.3gpp.org.